CONF-770766-17

PREPRINT UCRL- 79712

Lawrence Livermore Laboratory

RESPONSE OF POROUS BERYLLIUM TO STATIC AND DYNAMIC LOADING

W. M. Isbell, O. R. Walton, F. H. Ree

July 1977

MASTER

This paper was prepared for submission to the 6th AIRAPT International High Pressure Conference, Boulder, Colorado, July 25-26, 1977.

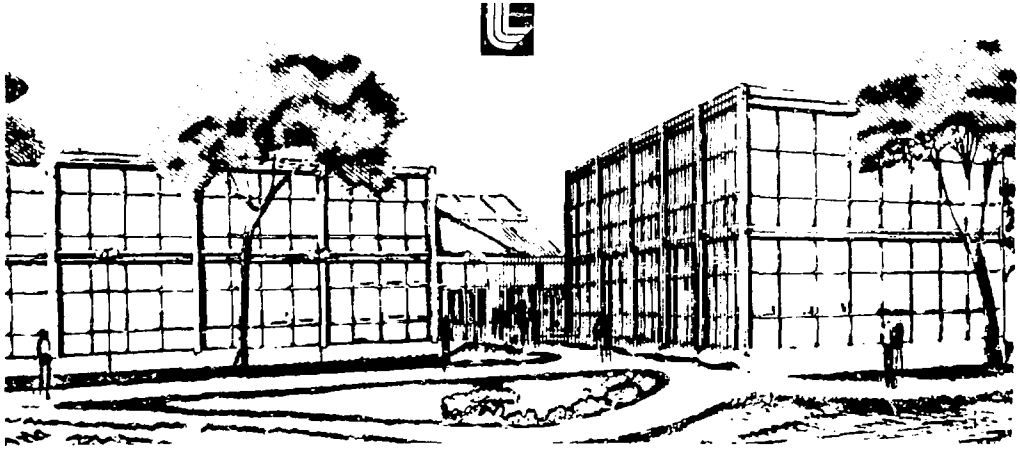

For Publication in the
Journal of Proceedings
6th AIRAPT
International High Pressure Conference
University of Colorado
Boulder, Colorado, USA
July 25-26, 1977

PAPER A-68

RESPONSE OF POROUS BERYLLIUM TO STATIC AND DYNAMIC LOADING*

W.M. Isbell**
O.R. Walton
F.H. Ree

Lawrence Livermore Laboratory
Livermore, California

ABSTRACT

Previous investigations of the mechanical response of porous materials to dynamic loading have been extended to include the shock wave response of a brittle metal. The complex response of berylliums of 85-90% porosity in two initial conditions has been examined in a theoretical and experimental program to be described. The study has resulted in the development of constitutive relations placed in hydrocodes which are capable of accurately predicting wave propagation in the berylliums. A comprehensive set of static (0 to 4 Gpa) and dynamic (0 to 35 Gpa) experiments was performed to measure the behavior of these brittle, porous materials to imposed loads. The results of the experiments guided a modeling effort which added several new features to

---

*Study supported by the Energy Research Development Agency

**Currently with Effects Technology, Inc., Santa Barbara, California

Work performed under the auspices of the U.S. Energy Research & Development Administration under contract No. W-7405-Eng-48.

previous models, including deviatoric stresses, porosity-dependent relaxation time of pore closure, elastic-plastic reopening of pores, and improved compaction functions.

FOREWORD

The effectiveness of porous materials in attenuating stress pulses and in reducing the thermomechanical stresses arising from rapid energy deposition has been the subject of numerous studies during the past decade. Because of the large number of manufacturing parameters (composition, porosity, pore size, heat treatment, etc.) available to the developers of porous materials, extensive tailoring of properties to meet widely varying requirements is practical and the materials manufactured and the studies to date now number in the dozens.

The present study involves two porous berylliums of different initial heat treatments and slightly different porosities. A theoretical model was developed and a series of measurements were made to describe the complex equation of state surfaces peculiar to porous materials. Hydrocode predictions, using this model, gave adequate comparison between theory and measurement.

EQUATION OF STATE SURFACE

Thermodynamic equilibrium properties of non-porous materials may be described by unique relationships between the thermodynamic variables pressure, temperature, entropy, energy, volume, etc. This unique relationship between the thermodynamic variables is often represented by a three-dimensional surface showing the allowed thermodynamic equilibrium "states" of the material in terms of any three of the thermodynamic quantities. Figure 1 shows a schematic representation of the pressure, temperature, and volume relationship for a typical material, including phase changes. Each point on this non-porous equation of state surface represents a unique state-point, i.e., the pressure at a particular volume and temperature is independent of the "path" (or past history) used to arrive at that volume and temperature.

No such unique relationship exists for porous materials. The complex non-equilibrium thermodynamic states that can be reached by a porous material are not described by a single equation of state, but rather by a mathematical model that depends on the thermodynamic path by which the material arrived at its current state. The porous "addition" to the surface shown in Figure 1 represents only an initial crushing surface. Unloading and subsequent reloading of the porous material occurs on another path which penetrates below the initial crushing surface. This is shown as an intermediate crush surface on the figure. Such intermediate crush surfaces are examples of how the pressure in a a porous material depends

not only on the volume and temperature, but also on the past history of the material.

DYNAMIC BEHAVIOR

The initial compaction surface (and the intermediate unloading-reloading surfaces) shown in Figure 1 is valid only for static or quasi-static loadings and unloadings. If the loading is rapid (as in a shock wave front for instance) then inertial and viscous resistance to the rapid collapse of the pores will come into play to make the dynamic compaction path lie above the quasi-static path. In both impact tests and energy deposition tests the initial stresses produce pore collapse rates that are very high. These high pore collapse rates lead to temporary overstresses.

Several models have been proposed[6-10] to describe rate dependent pore collapse. Most of these assume that a dynamic overpressure (dependent on the rate of pore collapse) exists for some characteristic time, τ, (dependent on material properties) with an exponential relaxation to the static crushing surface. Each of the models used can be calibrated, with varying degrees of success, to agree with the rise times and wave velocities from plate impact experiments.

THE POROUS CONSTITUTIVE MODEL

The model we have used to describe the porous beryllium [3] is based on Holt et al's P-α-τ model [7] which is in turn a rate-dependent modification of Herrman's model.[6] The new features in the present model

are: the inclusion of deviatoric stresses, the use of a porosity-dependent relaxation time for pore closure, an allowance for partial reopening of the pores on unloading, and the use of improved static compaction functions.

Two relations are used in the formulation of the constitutive model. The first relation is an equation which relates the pressure (P), volume (V), and energy (E) of a porous material to the equation of state (EOS) of the corresponding fully compacted solid. The porosity parameter α is defined by the relation:

$$P(V,E) = \frac{1}{\alpha} P_s\ (V/\alpha,\ E_s), \tag{1a}$$

which can be rewritten in an alternate but equivalent form,

$$\alpha = V/V_s = P_s/Pm \tag{1b}$$

where the subscript s refers to the solid material.

The second relation used in formulating the model is an equation which describes the elastic and plastic portion of paths for α during a time-dependent deformation process. Along the plastic path, we use the rate-dependent pore-closure relation of Holt et al.,

$$\alpha = g(P) - \tau\ d\alpha/dt. \tag{2}$$

The parameter τ is a time constant describing the rate of plastic flow of material into pores, which reduces α to a final average equilibrium

value given by the static compaction function g(P).

To determine g(P), we eliminate V in Eq. 1 by using hydrostatic P-V data for both solid and porous beryllium. The resulting data, P and g(P), can be accurately represented by the following expression:

$$g(P) = \alpha_\infty + (\alpha_0 - \alpha_\infty) \exp(aP + bP^2 + cP^3). \qquad (3)$$

where α_0 is the initial porosity and α_∞ is introduced to account for some residual porosity that appears to persist under extremely high pressures.[5,11] The constants a, b, and c are obtained by fitting the data by a least-squares method.

A modification of the elastic viscoplastic rate dependent behavior described by Holts spherical pore model is used to describe the rate dependence of the compaction. A porosity dependent τ (of equation 2) of the form

$$\tau = \tau_0 \alpha_0 (\alpha_0 - \alpha_\infty)/[\alpha(\alpha-\alpha_\infty)] \qquad (4)$$

can be calibrated to fit the calculated wave profiles for as-sprayed beryllium.

To obtain an equation for α along an elastic path, the porous and solid EOS's are expressed in incremental form. That is, using Δ to denote

the difference in P (and in P_s) at two successive time steps we have

$$\Delta P = K(\Delta\rho/\rho), \quad : \tag{5a}$$

$$\Delta P_s = K_s \ (\Delta\rho_\sigma/\rho_s) \ , \tag{5b}$$

where K and K_s are the bulk moduli of the porous and solid materials, respectively. After lengthy algebraic manipulation, we obtain an expression for the rate of change of α with P along the elastic path; i.e.,

$$d\alpha/dP = \alpha(K_s/K - \alpha)/(\alpha P - K_s) \tag{6}$$

where Mackenzie's [12] expressions for K and G are rewritten

$$1/K = (\alpha_\infty/K_s)t + (1/K_o) \ (1 - t) \ , \tag{7a}$$

$$G = (1/G_s)t + (1/G_o)(1 - t) \ , \tag{7b}$$

where

$$t \equiv (\alpha_o - \alpha)/(\alpha_o - \alpha_\infty) \ ,$$

and the subscript O refers to the initial porous state.

Yield Stress

To complete the formulation, the deviatoric stress s must be specified. Then, the axial stress σ_1 (along direction 1) in a 1-D

strain deformation is given by

$$\sigma_1 = -P + s_1 \ , \tag{8}$$

where

$$s_1 = \frac{4}{3} G \ln(V/V_o), \text{ if } |s_1| < \frac{2}{3} Y \ , \tag{9a}$$

$$= \pm \frac{2}{3} Y \text{ otherwise (+ for loading and - for unloading).} \tag{9b}$$

The shear modulus G in Eq. 9a is calculated from Eq. 7b. Y may be calculated from $\frac{2}{3} Y = \sigma_1 + P$ if experimental data are available for P and σ_1. The data can be fitted by a functional form such as

$$Y = \text{Max } [Y_o, Y_1 + Y_2 \varepsilon + Y_3 \varepsilon^2] \ , \tag{10}$$

where $\varepsilon = \ln(V/V_o)$ and small elastic strain is neglected.

DESCRIPTION OF THE POROUS BERYLLIUMS

Two porous beryllium materials were studied, both plasma-sprayed by Union Carbide Corporation from powders supplied by Kawecki Berylco Industries, Inc. The materials were prepared in accordance with Kaman Science Corporation specifications for Models 67 and 68 beryllium.

The plasma spraying process invoives the ejection of metallic powder using a jet of inert gas (argon) from a nozzle. The stream of powder passes through an electric arc and is melted to form a stream of molten droplets. These droplets land on a rotating aluminum mandrel

(or turntable). The nozzle moves radially in and out across the mandrel face during the spraying process so that the droplets form a spiral pattern in and out across the mandrel, building up a plate, layer upon layer.

Two grades of beryllium powder were used to manufacture the plates, P-1 and P-10. Specimens made from P-10 powder were tested in the "as-sprayed" condition while specimens from P-1 powder were sintered for 2 hours at 1175°C, producing a less porous and stronger material. Table I summarizes the chemistry of the two powders used and the densities of the resulting plasma sprayed materials.

TABLE I

		P-10 (-325 mesh, not sintered) (wt%)	P-1 (-325 mesh, sintered) (wt%)
Chemistry:	BeO	0.66	0.72
	Fe	0.075	0.035
	Al	0.024	0.006
	C	0.029	0.026
	Mg	0.026	0.002
	Si	0.010	0.008
Density:	gm/cm^3	1.587	1.647
Porosity:		14.2%	11.0%

EXPERIMENTAL DATA

To perform meaningful calculations, a computational model must first be fitted to accurate and reasonably complete experimental data. In the present study, impact and static pressure-volume data provided paths for mechanical loading and unloading and rate-dependency of yielding as well as providing a check on the calculational ability of the model to predict shock wave attenuation. Ultrasonic measurements were used to provide elastic moduli at standard temperature and pressure. Microscopic examination of compressed specimens yielded insight into deformation and mechanisms of the pore collapse process. Effective Gruneisen and expanded volume states were measured using an electron-beam machine to provide nearly constant-volume thermal heating in short deposition times.

A large amount of experimental data was generated on the two berylliums during this program. A brief synopsis of the data follows.

Static Compression Data

Throughout the study, quasi-static deformation data[2,13] served to guide the modeling effort. Considerable detail is contained in the data concerning:

- compression under hydrostatic and one-dimensional conditions
- release behavior of the compressed materials
- residual porosity at high pressures (> 4GPa)
- elastic yield in compression and release.

The relatively low cost of this data, when compared to shock wave data, makes the static technique an attractive alternative for characterizing porous materials. The static data, when combined with a modest number of shock wave tests to determine deviatoric and time-dependent behavior, has proven adequate for modeling several materials of interest.

Two types of experiments were performed: loading and unloading under conditions of uniaxial strain and under conditions of hydrostatic pressure. In uniaxial strain loading, an axial stress was applied to a cylindrical sample with the condition that the radial strain remain constant. This was achieved by control of the lateral confining pressure and resulted in a loading path similar, except for time-dependent flow, to that of plane shock-loading. In the hydrostatic testing an axial stress was applied to a medium surrounding a cylindrical sample. The plastic flow of the surrounding medium (fluid at low pressure and tin at high pressure) insured that the loading was almost hydrostatic in nature.

Details of the uniaxial strain loading data are shown in Figure 2. The inidial slope of the unsintered curve is seen to be much lower than in the sintered material, showing that the unsintered material is more compressible initially. This may be the result of some of all of the following effects:

- the sintering process, which produces more spherical and hence stronger pores
- the existence of numerous microcracks in the unsintered material

- the decreased porosity and thus greater strength in the sintered beryllium and
- the effect of residual stresses in the unsintered material, lowering the applied shear stress necessary to cause yielding.

Also shown in Figure 2 are Hugoniot points taken over the same stress range as the laboratory uniaxial data. Within experimental error, for the unsintered beryllium, the points are coincident with the path that defines the stress-volume curve. In contrast, the shock wave data for the sintered beryllium lie consistently above the static data, most probably indicating increased strain rate behavior for that material.

Shock Wave Tests

Shock wave generation and propagation under conditions of uniaxial strain were measured [1,5] using gas gun-launched impactors and a variety of experimental configurations. Data obtained included:

- Hugoniots to ~3.2 GPa (32 kbars)
- Release adiabats from shocked states
- Shock wave profiles for attenuated and unattenuated waves
- Compressional and release velocities over a range of stresses

A separate series of explosive tests [11] extended the range of Hugoniot measurements to over 33 GPa (330 kbars).

Most data were used directly in developing the material models, although independent check data (primarily attenuated wave profiles) were used to determine the accuracy of the model's predictive capability. This section summarizes the data obtained and experimental techniques used.

Hugoniot data and unattenuated wave profiles were obtained primarily with the three measurement techniques shown in Figure 3. A 90 mm diameter gas gun was used to launch four porous beryllium specimens into four materials of different impedances mounted on quartz stress gages (Figure 3a), or reversing the procedure, to launch four materials of different impedances into beryllium specimens mounted on quartz gages (Figure 3b).

The "direct impact" technique (a) provided Hugoniot data in the form of stress-particle velocity points calculated by knowledge of the Hugoniots of the four impactor materials plus the known characteristics of the quartz stress gages and buffers. This multiple gage technique is particularly efficient in reducing ambiguities among data points in that all specimens are impacted at the same impact velocity and at the same impact tilt. Cross correlation between data points is thus facilitated and results in relatively accurate data.

Although quartz stress gage measurement techniques have advantages in simplicity and reasonably well-known gage characteristics, the (usually) large change in shock impedance at the gage-specimen interface reflects a portion of the shock wave and may considerably complicate analysis. An ideal measurement technique would require in-situ measurement of the passage of the shockwave without disturbance of the wave itself. At present, "in-material" piezoresistive stress gages meet this requirement most closely.

Figure 4 shows Hugoniot data obtained to 4.5 Gpa (45 kbars). The relatively low compaction wave and high initial release wave velocities account for the very rapid attenuation rates customarily found in porous materials.

For most of the wave profiles used for model development and for checks on predictive capability, carbon-Kapton* in-material stress gages were used in the configuration shown in Figure 3c. Since the gage is quite thin (0.1 mm), it usually comes into pressure equilibrium with the specimen material within a few hundred nanoseconds by a series of shock reverberations across the gage, even though the shock impedances of the gage and test specimens may be very different. Thus if a suitable calibration has been performed on the gage, one obtains a direct measure of the stress in the test specimen. It should be noted, however, that the impedance difference does indeed affect the profile shape somewhat, and accurate work requires the ability to calculate profiles using equations of state of the gage and of the material under test.

*DuPont trademark

Using in-material gages placed between successive layers of the specimen, we studied the evolution of waves as they progressed through the material. Elastic and plastic compressive and release waves were measured, and by using careful timing techniques, wave speeds were obtained.

COMPARISON OF PREDICTIONS WITH DATA

Experimental wave profiles for comparison were obtained at two stress levels, approximately 0.6 and 1.7 GPa. Profiles were obtained by impacting a PMMA plate onto either sintered or as-sprayed porous beryllium having carbon-Kapton piezoresistive gages embedded at as many as six different depths within the material. Thus a single experiment took data on wave profiles at several different levels. The gages were located as deep as 1.9 cm from the impact surface and some measurement times extended up to 4 μs. The resulting 21 wave profiles-- both unattenuated and attenuated--represent large variations in the physical parameters and enabled us to extensively test the model.

Measured and computed wave profiles are compared in Figure 5 for the sintered material and in Figure 6 for the as-sprayed material. Agreement between the experimental wave profiles and those predicted from the present model is good both quantitatively and qualitatively.

For sintered porous beryllium (Figure 5) an elastic precursor about 0.4 GPa high, which corresponds to the "shoulder" in the hydrostat in Figure 2 precedes the main plastic wave. At the foot of the precursor the velocity is close to the longitudinal sound speed, but it becomes slower at higher stresses. The value 0.62 cm/μs at P = 0.2 GPa chosen for the calculation of the first arrival times agrees reasonably well with the velocity of the precuror at this level.

A faster-rising shock front, the lack of an elastic precursor, and a higher predicted attenuation rate are chief distinguishing features of compressive profiles in as-sprayed porous beryllium. Other tests at 1.7 GPa (17 kbars) showed similar behavior.

We also note from Figures 5 and 6 that the arrival times of the shocks (and their precursors in the case of sintered specimens) agree satisfactorily. The relaxation time τ = 0.04 μs matches the observed risetimes of the shocks in the case of the sintered specimens, while the porosity-dependent τ from Equation 4 adequately describes the risetimes of the shocks in the as-sprayed specimens. In the latter case, it is noteworthy that τ changes from 0.060 μs at the foot of the shocks to 0.015 μs at 1.7 GPa. If, instead of Eq. 4, a constant value (0.015 μs) had been used for τ, the foot of the shocks would be traveling too fast, resulting in much longer risetimes than those in the observed profiles.

The largest deviation occurs in the calculation of the peak stresses, with the experimental data lying 10% or less below computer predictions. Either experimental uncertainties or approximations in the model or a combination of the two could account for these relatively small differences.

SUMMARY

We have shown that significant differences exist between the porous as-sprayed and the sintered beryllium materials examined in this study. We have demonstrated that the wave propagation properties of both of the material tested can be described by the porous material model developed. Both the compressive characteristics (first-wave arrival time, risetime of shock, and peak stress) and the release characteristics (arrival time of release wave and general attenuated shape) of shocks have been reproduced satisfactorily for different stresses and pulse durations as well as for different thicknesses of the porous specimens. Slight deviations between the experimental and computed wave profiles lie mostly within the combined errors of the model and the experimental data.

REFERENCES

1. W. M. Isbell, O. R. Walton, and F. H. Ree, Lawrence Livermore Laboratory Report UCRL-51682, Part 1 (1977).

2. R. N. Schock, A. E. Abey, and A. G. Duba, Lawrence Livermore Laboratory Report UCRL-51682, Part 2 (1974).

3. F. H. Ree, W. M. Isbell, and R. R. Horning, Lawrence Livermore Laboratory Report UCRF-51682, Part 4 (1974)

4. J. E. Hanafee and E. O. Snell, Lawrence Livermore Laboratory Report UCRF-51682, Part 6 (1974).

5. R. R. Horning and W. M. Isbell, Rev. Sci. Instr., 46, No. 10, (1975) p 1374-79.

6. W. Herrman, Constitutive Equation for the Dynamic Compaction of Ductile Porous Materials, J. Appl. Physics, 40, 2490 (1969).

7. A. C. Holt, A. S. Kusubov, D. A. Young, and W. H. Gust, Thermo-mechanical Response of Porous Carbon, Lawrence Livermore Laboratory, Report UCRL 51330, (1973).

8. M. M. Carroll, A. C. Holt, Static and Dynamic Pore-Collapse Relations for Ductile Porous Materials, J. Appl. Phys. 43, 1626 (1972).

9. Butcher, "Numerical Techniques for One Dimensional Rate Dependent Porous Material Compaction Calculations, SC-RR-710112, Sandia Laboratories Report, April 1971.

10. L. Seaman, R. E. Tokheim, D. R. Curran, Computational Representation of Constitutive Relations for Porous Material, Stanford Research Institute, prepared for Defense Nuclear Agency, DNA 3412F, (May 1974).

11. W. H. Gust, private communication, Hugoniot points to 33.5 GPa.

12. J. K. Mackenzie, Proc. Phys. Soc. B63, 2 (1950).

13. R. N. Schock, A. E. Abey, and A. G. Duba, J. Appl. Phys., 47, (1976).

FIGURE CAPTIONS

Fig. 1. Schematic representation of the P-V-T relationships for "typical" solid and porous materials

Fig. 2. Comparison of quasi-static uniaxial stress-strain data on two porous beryllium with corresponding Hugoniot data.

Fig. 3. Schematic of the measurement techniques used to obtain Hugoniot data and the stress-time profiles of transmitted waves. a) Hugoniot points from four specimens launched into four quartz gages with buffer plates of various shock impedances. b) Four compressive wave profiles at different material thicknesses. c) Attenuating wave profiles measure with in-material piezoresistive gages.

Fig. 4. a) Hugoniot points and their analytical representations. b) Compaction wave speeds vs. Up obtained from Hugoniots and initial release wave velocities calculated using equations 3 and 7.

Fig. 5. Full and attenuated wave profiles for a low-stress test in sintered porous beryllium. Theoretical predictions are shown by solid lines. Velocity of the 0.124 cm thick PMMA impactor was 0.0262 cm/μs.

Fig. 6. Wave profiles for as-sprayed porous beryllium at a similar impact velocity. PMMA impactor thickness was 0.1245 cm and impact velocity was 0.0258 cm/μs.

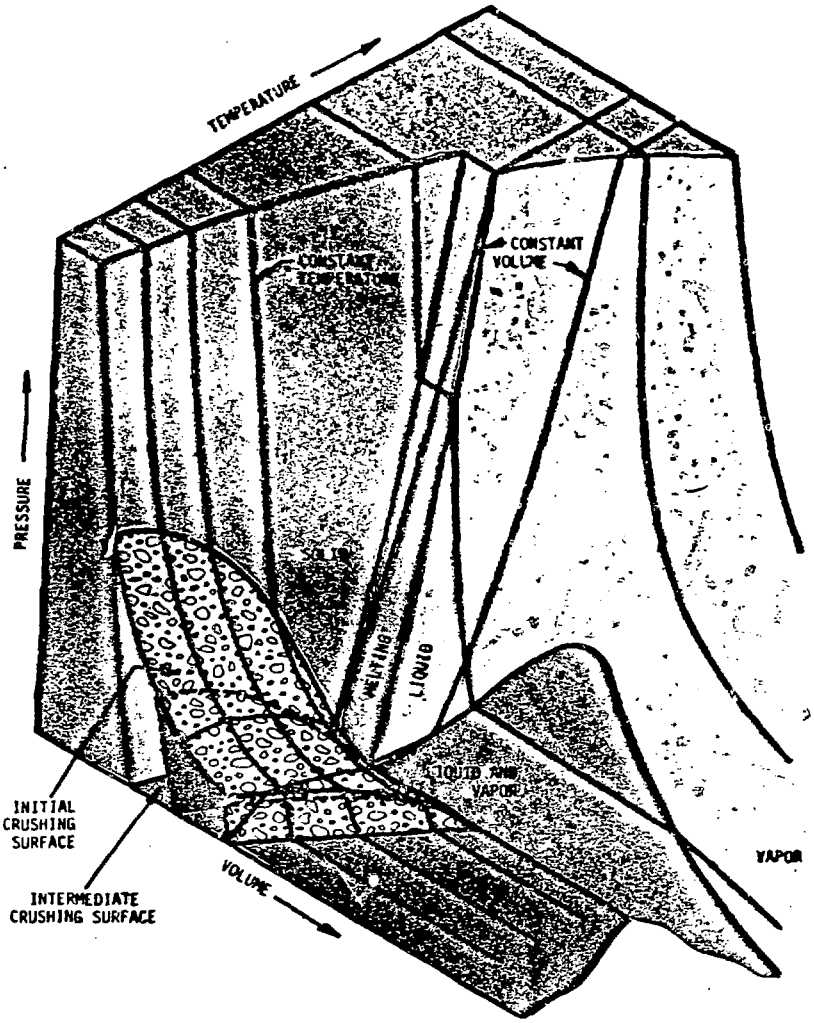

SUBJECT
NO.

FIG. 1

To be redrawn.

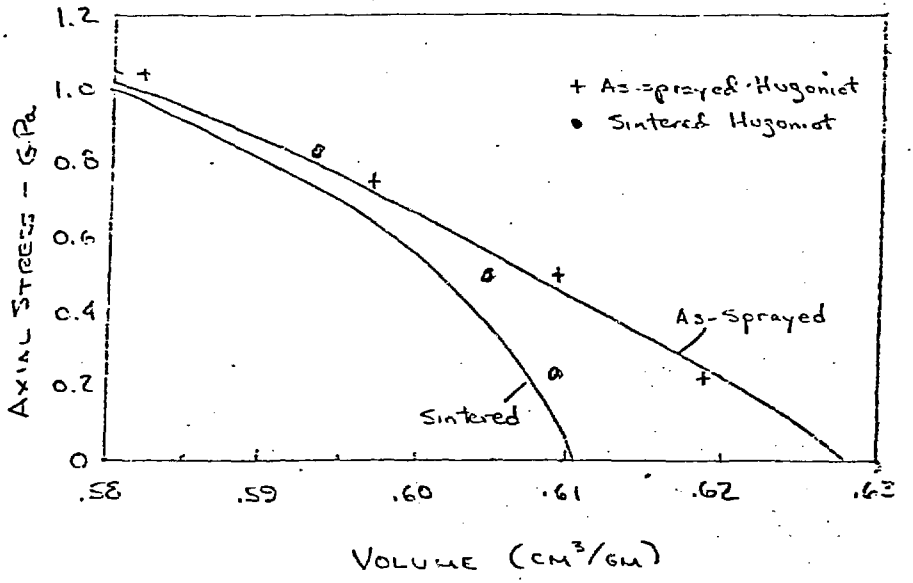

FIG. 8.1.1. COMPARISON OF AXIAL STRESS-STRAIN AND HUGONIOT DATA FOR TWO BERYLLIUMS

FIG. 2

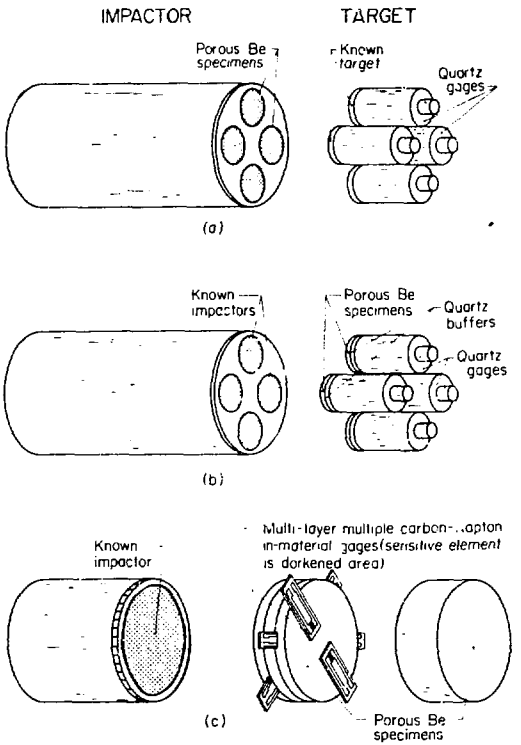
IMPACTOR
TARGET
Porous Be specimens
Known target
Quartz gages
(a)
Known impactors
Porous Be specimens
Quartz buffers
Quartz gages
(b)
Known impactor
Multi-layer multiple carbon-...apton in-material gages(sensitive element is darkened area)
Porous Be specimens
(c)

Fig. 3

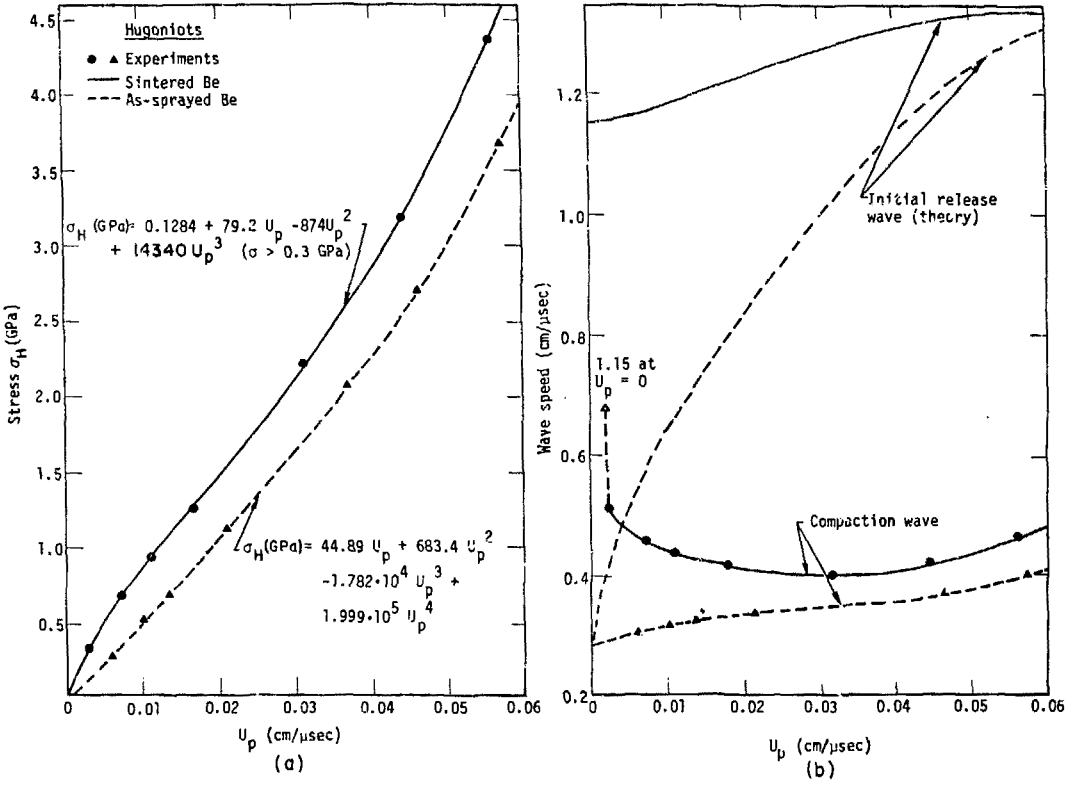
Hugoniots
● ▲ Experiments
Sintered Be
As-sprayed Be
σ_H (GPa)= 0.1284 + 79.2 U_p -874U_p^2 + 14340 U_p^3 (σ > 0.3 GPa)
σ_H(GPa)= 44.89 U_p + 683.4 U_p^2 -1.782·10^4 U_p^3 + 1.999·10^5 U_p^4
Stress σ_H (GPa)
U_p (cm/μsec)
(a)
Initial release wave (theory)
1.15 at U_p = 0
Compaction wave
Wave speed (cm/μsec)
U_p (cm/μsec)
(b)

Fig. 4

Fig 7

One-to-one

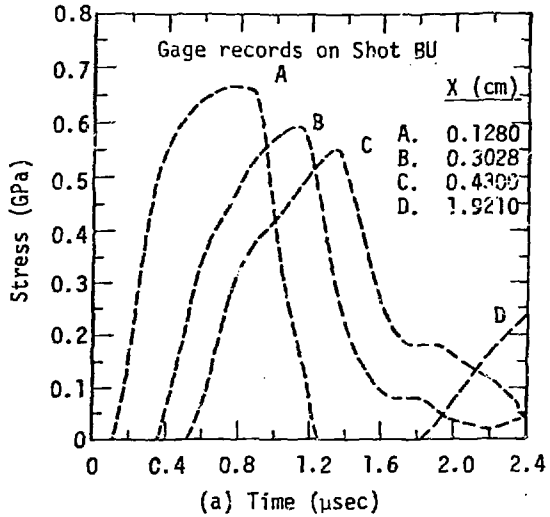

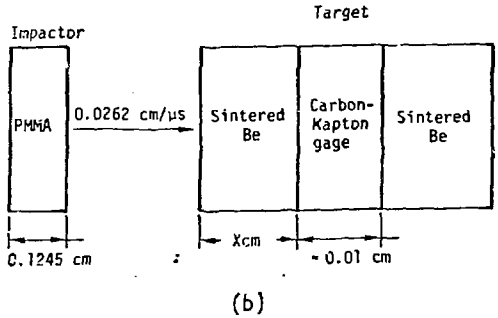

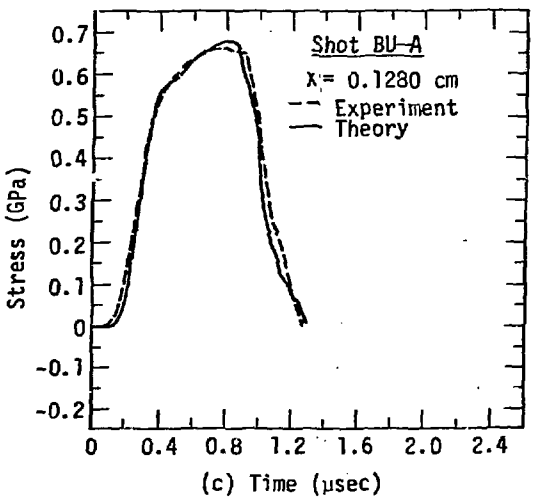

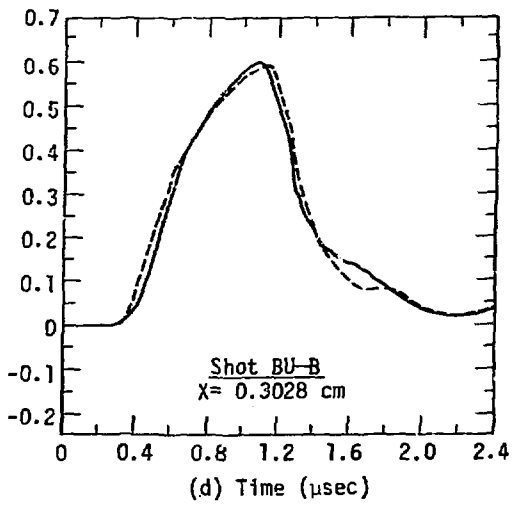

Fig 5

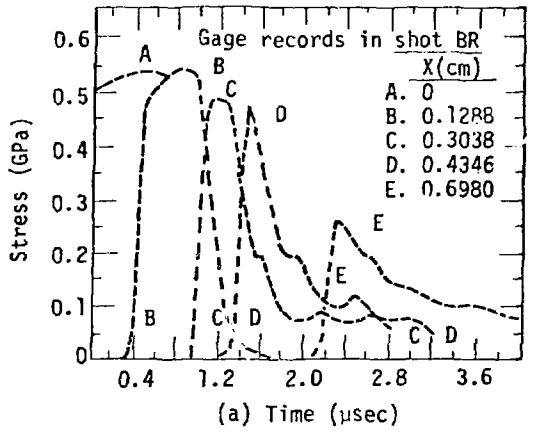
Gage records in shot BR
X(cm)
A. 0
B. 0.1288
C. 0.3038
D. 0.4346
E. 0.6980
Stress (GPa)
0.6
0.5
0.4
0.3
0.2
0.1
0
0.4
1.2
2.0
2.8
3.6
(a) Time (μsec)

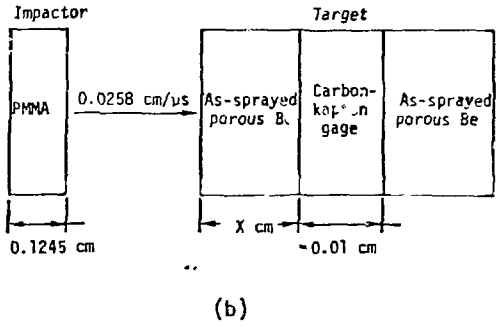
Impactor
Target
PMMA
0.0258 cm/μs
As-sprayed porous Be
Carbon-kapton gage
As-sprayed porous Be
X cm
0.1245 cm
~0.01 cm
(b)

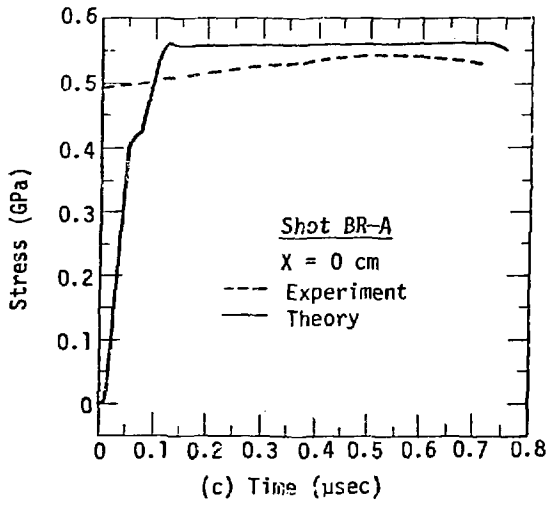
Shot BR-A
X = 0 cm
Experiment
Theory
Stress (GPa)
0.6
0.5
0.4
0.3
0.2
0.1
0
0 0.1 0.2 0.3 0.4 0.5 0.6 0.7 0.8
(c) Time (μsec)

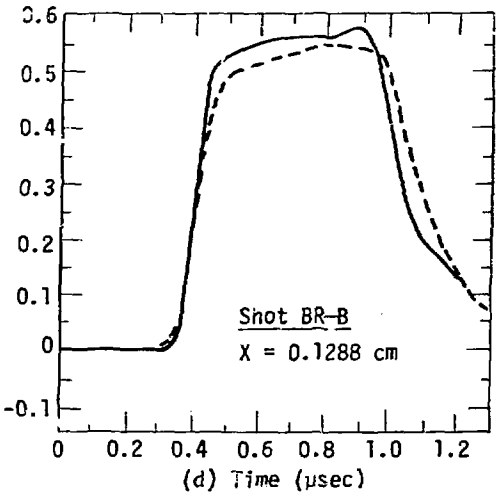
Shot BR-B
X = 0.1288 cm
0.6
0.5
0.4
0.3
0.2
0.1
0
-0.1
0 0.2 0.4 0.6 0.8 1.0 1.2
(d) Time (μsec)

FIG. 6